New energy-loss constraints on dark sectors from deeply inelastic scattering with initial state radiation

Justin Cammarota,[1,*] John Carlton,[1,2,†] and Susan Gardner[1,‡]

[1]*Department of Physics and Astronomy, University of Kentucky, Lexington, Kentucky 40506-0055, USA*
[2]*Deutsches Elektronen-Synchrotron DESY, Notkestrasse 85, 22607 Hamburg, Germany*

(Received 8 July 2026; accepted 28 September 2026; published 27 October 2026)

We employ the joint QED and QCD factorization of deeply inelastic, electron-proton scattering with generic initial state radiation to probe the possibility of exotic particle emission—i.e., of weakly coupled particles originating from a dark or hidden sector—through anomalous energy loss. We leverage this possibility through the consideration of phase-space-limited kinematic regions, for which the emission of an additional, undetected particle can particularly impact the associated cross section. In this first paper, as a proof of principle, we focus on radiation from the incoming electron, considering the modification of the lepton distribution function from the emission of particles, that could have spin of up to 2 and various, well-motivated electron couplings. We illustrate the sensitivity of our approach through the computation of the modified cross sections for the emission of MeV-GeV mass-scale, spin 0 particles in kinematics chosen for their sensitivity to initial state electron radiation and suitable to the forward-backward detection sensitivity of the ePIC detector at the Electron Ion Collider.

DOI: 10.1103/rjgy-fcr8

I. INTRODUCTION

We propose a new search strategy for as-yet-unknown light particles at upcoming accelerator facilities, such as the Electron Ion Collider (EIC). Despite much astrophysical evidence for dark matter, its particle nature and nongravitational dynamics continue to be unclear [1]. Moreover, the dynamical origin of the cosmic baryon asymmetry is not yet understood [2], and, with the discovery of gravitational waves [3], the prospects of identifying any footprints of quantum gravity beckon [4]. With these various motivations, searches for new particles, nominally of a hidden or dark sector, have long been conducted in experiments at accelerators, either through bump hunt or displaced vertex searches. Here we offer a new possibility: constraining the emission of light, weakly coupled particles through anomalous energy loss, i.e., through the determination of the modification of the cross section that their emission would generate. To realize this new "nonbump-hunt" strategy, we employ the joint QED and QCD factorization of deeply inelastic, electron-proton scattering [5–7] with generic initial state radiation (ISR) to study the possibility of exotic particle emission—of weakly coupled particles of varying mass and spin—that are undetected save for the energy loss they generate.

The new, combined factorization approach reduces the uncertainties associated with the computed radiative corrections to electron-hadron scattering in traditional treatments, such as that of Mo and Tsai [8–10] or of the Dubna group [11–13], due to the parameter-dependent corrections they incur, which vary with the implementation [14]. Generally, electroweak radiative corrections to deeply inelastic scattering (DIS), noting, e.g., [8–17], can potentially dominate the DIS cross section in regions with more limited phase space, such as at large y and Q^2. Under radiative corrections, the virtual photon can also develop a pinch singularity, which would need to be removed through a choice of kinematic cuts [7].[1] In the new factorization approach, these limitations are addressed and removed at a formal level, and the trade-off is the introduction of nonperturbative functions associated with initial- and final-state leptons in the scattering process to describe possible radiation beyond QED. These functions are not known exactly; however, they can be determined from the experimental data and their evaluation in some combination of lattice QCD with QED is an open possibility.[2] In this

*Contact author: justin.cammarota@uky.edu
†Contact author: john.carlton@desy.de
‡Contact author: susan.gardner@uky.edu

Published by the American Physical Society under the terms of the Creative Commons Attribution 4.0 International license. Further distribution of this work must maintain attribution to the author(s) and the published article's title, journal citation, and DOI. Funded by SCOAP³.

[1]Or, this can be regulated theoretically by either limiting the energy of the radiated photon, or by giving the virtual photon an infinitesimal mass.

[2]We note [18] for a review of existing approaches and applications. More work must be done to show these new nonperturbative functions can be calculated, possibly in analogy to lattice QCD computations of parton distribution functions (PDFs) [19].

way, the uncertainties in the joint QED and QCD factorization method can be controlled, and here we study their impact explicitly. A "QCD ⊗ QED" framework also exists [20–24], with different goals from the combined framework we use here, and we refer to Sec. II for details.

With the new QED and QCD framework in place, measurements of lepton-hadron DIS can be much more sensitive to energy-loss signatures, opening a new avenue to search for physics beyond the Standard Model (SM). The energy loss approach for detecting exotic particle emission that we espouse here can be applied broadly, though the range of possible particle dark matter masses is much broader still, ranging from as small as 10^{-22} eV, say, to 10^{15} eV or more [1]. Here we focus on the discovery prospects associated with the MeV-GeV mass scale, both because of the particular capabilities of the upcoming EIC and because that regime, at existing facilities, has proven challenging experimentally, leaving large swathes of unexplored parameter space [25,26]. Thus, the upcoming EIC, with a maximum $e-p$ center of mass energy of 140 GeV [27], provides an ideal setting for non-SM searches in the MeV-GeV mass region. In this paper we focus on the DIS cross section, in different final states and kinematics, but the study of other observables may well prove fruitful. For example, energy loss studies can take advantage of the recent developments in energy-energy correlators [28,29]; however, such a study is beyond the scope of this work.

A broad range of beyond the SM (BSM) physics can be studied in this manner, though in this first paper we focus on the impact of new particles that couple only to electrons. As long as the Lagrangian of the dark sector and its interactions with electrons is compatible with the SM, the contribution of the new particles to the DIS process can be computed in a manner similar to that of the SM radiative corrections in the QED and QCD factorization approach [5–7]. This work focuses on the corrections to the perturbatively calculable lepton distribution functions (LDFs) and fragmentation functions (LFFs), since, as in QED, the non-SM particles are presumed to be weakly coupled. More generally, nonperturbative models for the LDFs and LFFs can potentially also be determined [5–7], though this would require the use of experimental data. Archival DIS datasets typically have some QED radiative corrections applied to them, and they would have to be removed in order for the data to be used in the fitting process we envision. Here we use reference models in order to determine the observables that can minimize their effects.

In this work, in order to leverage the sensitivity of undetected, non-SM particle emission, we choose to study DIS with ISR from the incoming lepton line as our primary process, which is inspired by the use of ISR in e^+e^- collisions at KLOE to probe the running of the fine-structure constant α_{EM} [30]. In this paper, we also focus on the case in which the non-SM particle is also emitted from the incoming lepton, and this is possible because final-state radiation has a smaller overall effect on the cross section. This plan also takes advantage of the far detection capabilities planned for the EIC [27], and this motivates why we use its specifics to guide our kinematic choices. Most ISR, at least in the kinematics we consider, is collinear, and this makes it difficult to detect in the primary ePIC detector. However, the far detectors along the direction of the lepton beamline allow for direct measurements of the photon's energy, which should help with background suppression and make our desired candidate events more appreciable. This extra detection does require a slight modification to the QED and QCD factorization scheme we have mentioned; however, prior work has already shown how to address photoproduction in hadron collisions [31] and the leading-order approximations of that paper can be applied here.

We conclude this section by outlining the content of those to follow. First, we briefly summarize the standard QED and QCD factorization approach and provide its essential formulas. We then turn, in the following section, to a discussion of the sorts of non-SM particles of interest to us. If the new particles were massless, then Lorentz invariance would demand that their spin cannot be 3 or higher—and the massless spin 1 and 2 particles would couple via a conserved charge (e) and a universal graviton coupling, respectively [32]. Thus we reach beyond the photon and the graviton by considering massive particles. The spin 2 possibilities are especially interesting because of their connections to quantum gravity [4,33,34] as well. A broad range of candidates and candidate masses are possible, and in this paper, with our tilt to the capabilities of the EIC, we focus on candidates in the MeV-GeV mass range—and we develop detailed predictions for those with spin 0 only, for simplicity. Then, in the following section, Sec. IV, the DIS with ISR process is described in more detail, along with more discussion as to how to ensure its detection at the EIC. Subsequently, in Sec. V, we show how particular kinematic choices that yield large values of the radiative corrections also leverage the largest impact on the DIS + ISR cross section from undetected, non-SM scalar particle emission. Finally, we conclude with a summary and outlook.

II. QED AND QCD FACTORIZATION

DIS cross sections have long been calculated by separating contributions from process-dependent terms and process-independent terms through a controllable approximation method called (QCD) factorization [35]. This requires two scales to distinguish between the hard and soft parts of the scattering process, or particularly that $Q^2 \equiv -(\ell-\ell')^2 \gg \Lambda^2_{\mathrm{QCD}}$ in the DIS process $e(\ell)h(P) \to e(\ell')X$. To describe the behavior of partons inside the hadron with their longitudinal momenta, PDFs are used to characterize the nonperturbative nature of the quarks and gluons [36].

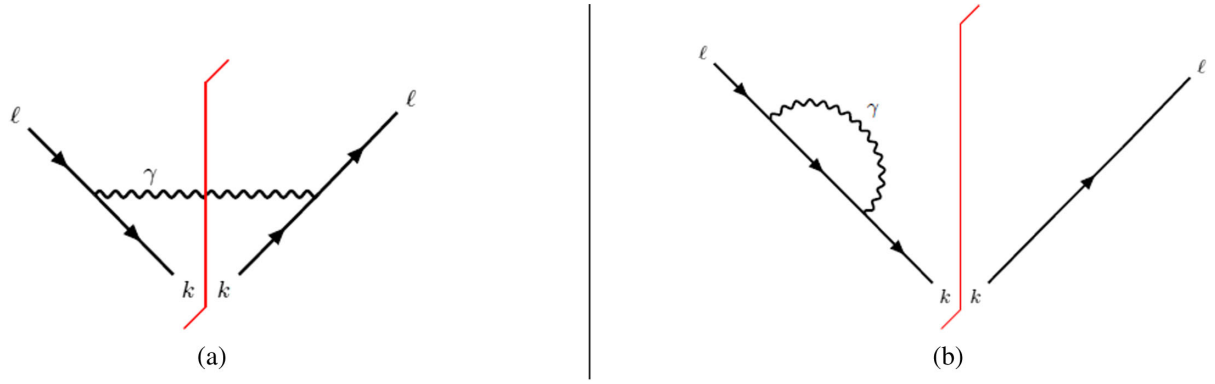


FIG. 1. The $\mathcal{O}(e^2)$ cut graphs [37] for the (a) real and (b) virtual contributions to the LDF associated with $e(\ell)h(P) \to e(\ell')X$, where in (b) the Hermitian conjugate must also be included.

Unobserved lepton radiation can drastically shift the cross section for lepton-hadron scattering processes, such as DIS, since the collision-induced lepton radiation changes the internal momentum transfer. The radiation can also alter the direction of the exchanged momentum, which means the expected Breit frame used to assess the cross section (thus defining the PDFs) is different from the actual one the particles would possess. The new QED and QCD factorization method [5,6], that we use here, puts QED and QCD radiation on an equal footing and removes this mismatch—and it also eliminates the pinch singularity coming from the exchanged photon, that we had noted earlier. The lepton analogs of the PDFs and parton fragmentation functions (FFs) for the quarks, the LDFs and LFFs, are defined for the incoming and outgoing leptons, respectively. This approach considers all QED radiation at the partonic scattering level and factorizes the collinear sensitive radiation into the LDF for leptons and PDFs for quarks (similarly for final state radiation into LFFs and FFs) [7].

The LDFs and LFFs can contain hadronic contributions, in principle, and thus nominally are nonperturbative objects. However, if those, such as could arise from a radiated photon splitting to a $q\bar{q}$ pair that could also scatter with other quarks, are neglected, then the LDFs (and LFFs) become purely QED functions—and are perturbatively calculable in powers of e. The perturbative and nonperturbative LDFs (and LFFs) are treated as independent functions [7], and we refer to Sec. V for a discussion of their modeling and their impact on our analysis. We focus on the energy loss from ISR, so that the LDFs enter here, but the LFFs would be constructed similarly, and we refer to [5–7] for further discussion. With $\xi = k^+/\ell^+$, as per the notation of Fig. 1 and in light cone coordinates[3] at leading order (LO), $f^{(0)}_{e/e}(\xi) = \delta(\xi - 1)$, which is intuitive as in this case there is no lepton-induced radiation. A vertical, broken line in Fig. 1 indicates a "cut" graph, where propagators crossing the cut are placed on their mass shell, and we refer to [37] for all details. In next-to-leading order (NLO), $\alpha_{\rm EM}$ appears explicitly in the LDF, and this feature will become key when we turn to the analysis of non-SM particle emission. The NLO contributions can be calculated from the Feynman diagrams in Fig. 1 in light cone gauge, i.e., $A^+ = 0$ [36,38,39], as computed in [5,6], and the result in leading logarithmic order is

$$f^{(1)}_{e/e}(\xi,\mu^2) = \frac{\alpha_{\rm EM}}{2\pi}\left[\frac{1+\xi^2}{1-\xi}\ln\frac{\mu^2}{(1-\xi)^2 m_e^2}\right]_+, \tag{1}$$

where the "+" prescription in the standard convention is

$$[f(x)]_+ = f(x) - \delta(x-1)\int_0^1 \mathrm{d}x f(x) \tag{2}$$

and μ is the factorization scale. The LDF combines with other functions, both hard and soft, to give the factorized DIS cross section, and this final quantity does not depend on μ. This can be seen by enforcing

$$\frac{\mathrm{d}\sigma_{e(\ell)h(P)\to e(\ell')X}}{\mathrm{d}\ln\mu^2} = 0, \tag{3}$$

which yields evolution equations, similar to the DGLAP equations for the PDFs [40,41]. For the LDF we have

$$\frac{\mathrm{d}f_{e/e}(\xi,\mu^2)}{\mathrm{d}\ln\mu^2} = \int_\xi^1 \frac{\mathrm{d}\xi'}{\xi'} P_{e/e}\left(\frac{\xi}{\xi'},\alpha_{\rm EM}(\mu^2)\right) f_{e/e}(\xi',\mu^2), \tag{4}$$

which evolves the LDF from an initial factorization scale that combines to remove the overall μ dependence [5–7]. Here $P_{e/e}$ is the evolution kernel, which is perturbatively calculable in a power expansion of $\alpha_{\rm EM}$ under QED alone [6], while an expansion in terms of both $\alpha_{\rm EM}$ and α_S is possible if the factorization scale is sufficiently large [7]. The factorization scale is conventionally chosen to be

[3]We use the convention $v^\pm = (v^0 \pm v^3)/\sqrt{2}$ for a generic vector v; here the $\hat{\mathbf{3}}$ direction points in the direction of the incoming lepton's momentum.

$\mu^2 = Q^2$, but the transverse momentum of the outgoing lepton, $\mu^2 = \ell_T'^2 = (1-y)Q^2$, is also a valid choice [5–7]. Because we are working in a collinear factorization approach, the $\ell_T'^2$ must be large also, which is normally correlated to the large Q^2 conventionally chosen.[4]

The factorized DIS cross section with only leading, process-independent QED radiative contributions is given by

$$E' \frac{\mathrm{d}^3\sigma^{\mathrm{RC(LO)}}_{e(\ell)h(P)\to e(\ell')X}}{\mathrm{d}^3\ell'} \approx \frac{1}{2s}\int_{\zeta_{\min}}^1 \frac{\mathrm{d}\zeta}{\zeta^2} D_{e/e}(\zeta,\mu^2) \int_{\xi_{\min}}^1 \frac{\mathrm{d}\xi}{\xi} f_{e/e}(\xi,\mu^2) \times \sum_q \int_{x_{\min}}^1 \frac{\mathrm{d}x}{x} f_{q/h}(x,\mu^2)\widehat{H}^{(2,0)}_{eq\to eX}(\hat{s},\hat{t},\hat{u}), \tag{5}$$

and is labeled "RC(LO)." We have already noted the LDF $f_{e/e}(\xi,\mu^2)$, and $D_{e/e}(\zeta,\mu^2)$ is the LFF, the function in the final state analogous to it. Generally, the function $\widehat{H}^{(a,b)}_{eq\to eX}$ describes a contribution to the hard scattering, partonic DIS process $eq \to eX$ in terms of powers of its coupling constants, namely, α^a_{EM} and α^b_S. Here $\widehat{H}^{(2,0)}_{eq\to eX}$ describes its first nonzero term in that power counting, thus giving the LO contribution to the cross section. Generally, the hard function $\widehat{H}^{(a,b)}_{eq\to eX}$ can contain μ dependence from its renormalization, but the leading term $\widehat{H}^{(2,0)}_{eq\to eX}$ is finite and no such dependence appears.

In this paper we work no higher than $\mathcal{O}(\alpha^2_{\mathrm{EM}})$. As we extend this framework to BSM physics, the cross section expression can be generalized to include other couplings, such as would come from BSM-particle-fermion couplings. The relationship in Eq. (5) is only approximate, because the LDFs and LFFs are expanded to work through NLO as we have described, though we will model and include their nonperturbative contributions separately, as discussed in Sec. V. In contrast, the PDF is a fully nonperturbative function determined from experimental data. As this is a factorized cross section, there are also higher-order contributions at the presumed factorization scale, though these are suppressed as $\mathcal{O}(\Lambda^2_{\mathrm{QCD}}/Q^2)$.

In Eq. (5), there are three integrations over the momentum fractions considered in the partonic scattering process. The first describes how the internal momentum k'^+ of the outgoing lepton produced in the scattering process is carried to that of the final-state observed lepton ℓ'^+, and $\zeta = \ell'/k' \approx \ell'^+/k'^+$. The second is the fraction of the initial-state lepton momentum entering the partonic interaction, that we have already defined. The last is the hadronic momentum fraction, following the standard definition for PDFs, $x = p^-/P^-$, where p is the momentum of the quark in the partonic scattering process in the CM frame, recalling ℓ is chosen to be in the $+$ direction, and P is that of its proton. The lower limits of integration are determined from the computed form of $\widehat{H}^{(2,0)}_{eq\to eX}$ and the Mandelstam variables $s = (\ell + P)^2$, $t = (\ell - \ell')^2$, and $u = (\ell' - P)^2$, with hatted variables denoting their partonic counterparts ($\hat{s} = (k+p)^2$, $\hat{t} = (k-k')^2$, $\hat{u} = (k'-p)^2$, where QED radiation from the quarks is implicitly absorbed in the PDFs), and noting $x_B = Q^2/sy$ and $y = (P\cdot q)/(P\cdot\ell)$. The kinematic limits, since the momentum fractions cannot be larger than 1, are explicitly given by [6,7]

$$\zeta_{\min} = -\frac{t+u}{s} = 1-(1-x_B)y,$$
$$\xi_{\min} = -\frac{u}{\zeta s + t} = \frac{1-y}{\zeta - x_B y},$$
$$x_{\min} = -\frac{\xi t}{\xi\zeta s + u} = \frac{\xi x_B y}{\xi\zeta + y - 1}, \tag{6}$$

where we have assumed $s, u \gg m_e^2 + m_p^2$ and $t \gg m_e^2$ throughout.

For completeness, we note that other groups have worked to combine QCD and QED effects to hadronic interactions through so-called QCD ⊗ QED frameworks, where they tend to focus on the resummation of logarithmic terms for the mixed contributions to the transverse momentum spectrum, especially for W and Z production in Drell-Yan at hadron colliders [20–23]. There has also been work that includes QED corrections to the Altarelli-Parisi splitting functions [42,43] and to realize mixed-order corrections to solutions to the DGLAP equations [24]. The joint factorization method discussed here is different, as it places QED and QCD radiation in hadronic contributions on the same footing—and it is not limited to the transverse momentum resummation formalism.

III. EXTENSIONS TO BSM PHYSICS

We open with a survey of how new particles, from physics beyond the SM, may couple to SM fermions. Although our initial focus is on the case of BSM particles that couple to electrons, we wish to describe a sweep of possibilities in order to set the stage for later work. The observation of a cosmic baryon asymmetry, of dark matter, and of direct evidence for the existence of gravitational waves—effects that are not of the SM of particle interactions—speak to the possibilities of new particles and forces, and the possible interactions they may have can depend on the dynamical function that they would possess. Since our new framework opens the possibility of probing new physics through energy loss in $e + p \to e + p + X$ scattering, we consider new particles of integer spin, even if

[4]Near the boundaries of the kinematic region, such as large y and low Q^2 (~1 GeV^2), this does not hold, see [7] for details.

new particles in the MeV-GeV mass range, such as dark matter, could be fermions. These bosons may be portals to extended dark sectors, gauge bosons of new fundamental forces and as such may kinetically mix with existing force carriers in the SM.

A. Electron and dark-sector particle interactions

We adopt an effective field theory approach to describe couplings between these new dark degrees of freedom and the SM, considering the broadest class of models. The primary consistency conditions we highlight are Lorentz invariance, gauge invariance, and unitarity. However, more subtle restrictions on theory parameter space also emerge from positivity bounds.

Restricting ourselves to Lorentz invariant operators of the lowest dimension, the permitted interactions depend on the spin and parity of the new field such that for a field χ, the interaction Lagrangian takes the form

$$\mathcal{L}_{\rm int} \supset g_\chi \chi \mathcal{O}_e. \tag{7}$$

Here, $\mathcal{O}_e$ is the electron bilinear matching the Lorentz structure of the dark matter field χ, and g_χ controls the coupling strength and production rate.

As we highlight in the introduction, the only viable massive Lorentz invariant fields we consider adding are spin 0, spin 1, and spin 2 [32]. In the following subsections we review each of these classes of model and how viable they are as dark matter candidates. In addition to spin, parity provides a useful classification of possible mediators. For each spin assignment we consider both parity-even and parity-odd states whenever allowed. This leads to six representative scenarios for J^{PC}: scalar (0^+), pseudoscalar (0^-), vector (1^-), axial-vector (1^+), tensor (2^+), and pseudotensor (2^-). These cases provide a model-independent framework for studying missing-energy signatures in this work. We summarize the effective couplings in Table I.

A new scalar degree of freedom is perhaps the simplest additional field to incorporate into the SM. The lowest dimension couplings couple to the electron bilinears given by $\bar{\psi}_e \psi_e$ for a scalar field ϕ and $\bar{\psi}_e i\gamma^5 \psi_e$ for a pseudoscalar a. Such candidates arise naturally in models containing additional Higgs-sector singlets, dilatons, and axionlike particles [44–46], with important constraints, particularly on axionlike particles, coming from astrophysics and cosmology [45,47]. While axions and axionlike particles are often thought of at lighter masses than the ones we consider in this work, there is nonetheless motivation to consider these heavier scalar candidates.

A massive spin 1 state A'_μ may couple either to the conserved vector current $\bar{\psi}_e \gamma^\mu \psi_e$ or to the axial current $\bar{\psi}_e \gamma^\mu \gamma^5 \psi_e$ [48,49]. The vector case includes dark-photonlike scenarios arising from kinetic mixing with hypercharge, while the axial-vector interaction can emerge from a broken U(1) symmetry with chiral charge assignments. Since both currents are dimension three, the resulting interactions are renormalizable and constitute the dominant low-energy couplings of a massive vector mediator to electrons.

TABLE I. Dark sector candidates considered as possible modifications to the LDF and their electron interaction Lagrangians.

Model	J^{PC}	Electron interaction Lagrangian
Scalar	0^+	$g_{se}\phi\bar{\psi}_e\psi_e$
Pseudoscalar	0^-	$g_{ae}a\bar{\psi}_e i\gamma_5\psi_e$, $g_{ae}\partial_\mu a\bar{\psi}_e\gamma^\mu\gamma_5\psi_e/2m_e$
Axial-vector	1^+	$g_{A'_x e}\bar{\psi}_e\gamma^\mu\gamma_5\psi_e A'_{x\mu}$
Vector	1^-	$g_{A'e}\bar{\psi}_e\gamma^\mu\psi_e A'_\mu$
Tensor	2^+	$g_{Te}h^{\mu\nu}\bar{\psi}_e\gamma_{(\mu}D_{\nu)}\psi_e$
Pseudotensor	2^-	$g'_{Te}h^{\mu\nu}\bar{\psi}_e\gamma_{(\mu}\gamma_5 D_{\nu)}\psi_e$

At leading order we expect a massive spin 2 field $h^{\mu\nu}$ to couple to the electron energy-momentum tensor $h^{\mu\nu}T_{\mu\nu}$. This reduces to the tensor couplings shown in Table I [50–52]. We also include a parity-odd tensor interaction term as a phenomenological effective field theory benchmark with an additional γ^5 term in the coupling. However, no symmetric rank-2 tensor exists in the Standard Model to generate this coupling in analogy to $T_{\mu\nu}$, making the parity-even coupling better motivated for study.

Theories of spin 2 dark matter, and therefore of gravitons and gravitonlike particles, are less well defined in a field theory language. Without a complete description of quantum gravity, we instead rely on effective theories to describe the behavior of a hypothetical spin 2 field to address at least some of the pathologies. This can be achieved by considering a more concrete nonlinear theory such as dRGT massive gravity [4] or by breaking more fundamental symmetries such as Lorentz invariance [53–55].

In this work we restrict ourselves to considering only Lorentz invariant fields as new degrees of freedom. Thus we employ the effective field theory of dRGT couplings of a massive spin 2 field (of mass m) with the lowest energy (high energy) cutoff scale given by $\Lambda_3 = (m^2 M_{\rm Pl})^{1/3}$. However, for an experiment performed on Earth we may instead use the redressed scale $\Lambda_* \sim 10^7 \Lambda_3$ (at the surface of the Earth), due to the Vainshtein mechanism changing the scale at which fluctuations become strongly coupled [4,56,57]. For a dark-sector particle mass on the order of MeV to GeV, we thus expect a cutoff of $\Lambda_* \sim (10^{10}$–$10^{13})$ GeV, which ensures the validity of considering these couplings in our work. The undressed cutoff Λ_3 would also be sufficient at the

energies we consider. Thus it may be possible to probe the validity of the Vainshtein mechanism through the effective spin 2 couplings we consider.[5]

Positivity bounds restrict self-interactions of massive tensor fields, but these align closely with the cutoff scale. Thus our effective theory remains valid for what we consider in this work [58]. No pseudotensor analogy of dRGT currently exists. However, we assume such an effective theory would have a similar cutoff scale.

B. Chiral basis

The spin 0 and 1 interactions of Table I can be captured in a compact way through the use of a chiral basis. Recalling that L^a and ℓ^b are the left-handed doublets and right-handed singlets of leptons in the SM, with $P_{R,L} = (1 \pm \gamma_5)$, we write, after [26],

$$\mathcal{L}_{\rm int} = \mathcal{V}_\mu [g^{ab}_{L\mathcal{V}} \bar{L}^a \gamma^\mu P_L L^b + g^{ab}_{R\mathcal{V}} \overline{\ell}^a \gamma^\mu P_R \ell^b], \tag{8}$$

where $\mathcal{V}_\mu \in (A'_\mu, A_{{\rm x}\mu}', \partial_\mu \phi/2m_e, \partial_\mu a/2m_e)$ and a, b are generational indices. Although $(L^b)^T = (\nu^b, e^b)_L$, we do not consider neutrino interactions in this paper. Since we are assuming parity invariance for simplicity, two sets of couplings, associated with $P = +$ or $P = -$ mediators, are of interest, namely,

$$\begin{aligned} g^{ab}_{L\mathcal{V}} &= g^{ab}_{R\mathcal{V}} \equiv g^{ab}_{\mathcal{V}_+}, \\ g^{ab}_{L\mathcal{V}} &= -g^{ab}_{R\mathcal{V}} \equiv g^{ab}_{\mathcal{V}_-}, \end{aligned} \tag{9}$$

with $\mathcal{V}_+ \in A'_{\rm x}, s$ and $\mathcal{V}_- \in A', a$. The terms in $\mathcal{L}_{\rm int}$ are each of mass dimension 5, but after integrating by parts and using the Dirac equation, we find the interactions for the scalar and pseudoscalar candidates we use here. Setting aside the possibility of charged lepton flavor violation, we let $a = b$ and consider electrons only henceforth—and we focus on the pseudoscalar case in what follows.[6] We might suppose that the use of either dimension 4 or 5 interaction terms would be *equivalent*. Yet there has been much discussion of this point in the literature, where we note [59] for a detailed exposition, with the outcome that our simple derivation is only approximate—and that differences between the two forms of the interaction can appear beyond leading order in the coupling constant. In the MeV-GeV region of interest to us, the possible coupling constants need not be negligibly small, and experimental investigations of the differences may be possible. Thus we pause to flesh out the issues concretely.

[5]It is worth noting that as this spin 2 massive particle is not the graviton, the cutoff scale of the theory is not necessarily controlled by the usual Planck mass, instead this is a free parameter. However, $M_{\rm Pl}$ is a natural choice for new physics to enter in the gravity sector.

[6]We note that electromagnetic current conservation forbids a term of form $\partial_\mu \phi \bar{\psi} \gamma^\mu \psi$.

The dimension 5 form of the $a - e$ interaction reveals that the physics should not change under a constant shift of the fields a. Such a shift symmetry is not apparent in the noted dimension 4 term, however, and here we show how to connect the dimension 4 and 5 forms precisely. Moreover, the fermion mass also plays a key role [60], as it is a particular feature of the pseudoscalar case. Writing $\tilde{g}_{ae} = g_{ae}/2m_e$, the Lagrangian for an electron ψ in the SM with an electron-axion interaction is

$$\mathcal{L}_{\rm fa} \supset \bar{\psi}(i\gamma^\mu D_\mu - m_e)\psi + \tilde{g}_{ae} \partial_\mu a \bar{\psi} \gamma^\mu \gamma_5 \psi, \tag{10}$$

Here $D_\mu \equiv \partial_\mu + ieA_\mu$ if e is the electron's physical charge. After redefining the fermion field as per

$$\psi \to e^{-i\tilde{g}_{ae} a \gamma_5} \psi, \tag{11}$$

we find, for the axionlike case, that [59,61]

$$\mathcal{L}_{\rm fa} \supset \bar{\psi}(i\gamma^\mu D_\mu - m_e e^{2i\tilde{g}_{ae}\gamma_5 a})\psi - \frac{\alpha}{2\pi} \tilde{g}_{ae} a F_{\mu\nu} \tilde{F}^{\mu\nu}. \tag{12}$$

The second term arises if $m_e \neq 0$ from the nonconservation of the axial vector current at the quantum level, due to the Adler-Bell-Jackiw anomaly [62–64]. Were we to ignore the impact of the chiral anomaly, we see that the two interactions would be equivalent to those in Table I in linear order of the coupling—but otherwise differ. The term that arises from the chiral anomaly in the axion case requires special treatment in our framework, because although it can contribute as radiation from the electron in the initial state, via $\gamma^* \to a\gamma$, this process is not collinear so that it cannot be ascribed to the perturbative LDF $f_{e/e}(\xi, \mu^2)$. This process, however, can contribute to the nonperturbative LDF. Thus we have shown that there is another role for BSM physics to play in the construction of this nonperturbative function, which we reserve for future work. Now we turn to the assessment of the LDF under (collinear) BSM particle emission.

C. Modifying the LDF with BSM physics

Under the joint QED and QCD factorization framework, BSM particle emission can easily be introduced through the modification of the LDF and LFF, using the interactions listed in Table I. Here, the LDF can now include the emission of a scalar or an axionlike particle, as shown in Fig. 2. Following [37], which also analyzes scalar emission from a fermion, we find for the real contribution to the emission of a scalar with mass m_S that

$$f_R^{(1),{\rm s}}(\xi, \mu^2) = \frac{g_{se}^2}{16\pi^2}(\xi - 1)\left[\frac{\xi(m_S^2 - 4m_e^2)}{(1-\xi)^2 m_e^2 + \xi m_S^2} - \ln\left(\frac{\mu^2}{(1-\xi)^2 m_e^2 + \xi m_S^2} + 1\right)\right]. \tag{13}$$

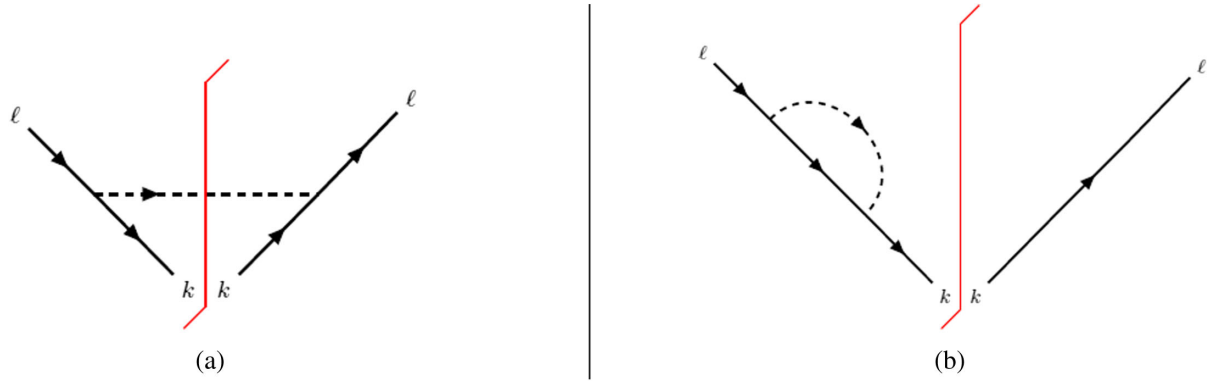


FIG. 2. Cut graphs for the Feynman diagrams for the $\mathcal{O}(g_{se}^2)$ real (a) and virtual (b) contributions to the LDF from a scalar, where the Hermitian conjugate of (b) also contributes.

Following the same method, we can compute the LDF for the axionlike case (with mass m_A) using the dimension 4 interaction of Table I to yield

$$f_R^{(1),\mathrm{a}}(\xi,\mu^2)=\frac{g_{ae}^2}{16\pi^2}(\xi-1)\left[\frac{\xi m_A^2+2(1-\xi)(m_e^2)}{(1-\xi)^2m_e^2+\xi m_A^2}-\ln\left(\frac{\mu^2}{(1-\xi)^2m_e^2+\xi m_A^2}+1\right)\right]. \tag{14}$$

Thus we see that the two functions are distinct. However, if we employ the leading logarithm approximation, as we did in the QED case, then those differences disappear. One expects this approximation to give the numerically dominant contribution to the cross section, because it controls end point effects from the ξ integration under the $+$ distribution. Finally, then, for the two cases, after combining the real and virtual contributions (which introduces the "+" prescription) and taking the leading logarithm approximation, we have

$$f^{(1),0}(\xi,\mu^2)=\frac{g_{ae}^2}{16\pi^2}\left[(1-\xi)\ln\left(\frac{\mu^2}{(1-\xi)^2m_e^2+\xi m_A^2}\right)\right]_+. \tag{15}$$

Following a similar process for the LFF case, where here $k^+=(1/\zeta)\ell'^+$, the leading logarithm approximation gives

$$D^{(1),0}(\zeta,\mu^2)=\frac{g_{ae}^2}{16\pi^2}\left[(1-\zeta)\ln\left(\frac{\zeta^2\mu^2}{(1-\zeta)^2m_e^2+\zeta m_A^2}\right)\right]_+ \tag{16}$$

for both scalar and axionlike particle radiation. We think these degeneracies emerge as a consequence of the properties of the parity transformation on the light front. Since the spatial coordinate in the $\hat{\mathbf{3}}$ direction of a vector $\boldsymbol{d}$ is used to construct $d^{+,-}$, a suitable construction of the light-front parity operator on d yields $d^{\pm}\to d^{\pm}$ and $d^{L,R}\to -d^{R,L}$, with $d^{L,R}\equiv d^1\pm id^2$ [65]. Since our results do not depend on the transverse coordinates, we suppose that is why the LDF (and LFF) for each case turn out to be the same.

IV. DIS WITH ISR

Motivated by the sensitivity of the DIS cross section to radiative corrections near the boundary of the kinematic phase space [5–7], we leverage its sensitivity to energy loss from BSM particle emission through the inclusion of SM ISR, such as that of a GeV-scale photon. Since the emitted BSM particles are undetected, experimental constraints on their mass are indirect.

Here we find that by measuring GeV-scale ISR, we can produce a kinematically restricted region that, in turn, is very sensitive to the emission of a leptophilic scalar and can also limit its mass. We note that the far-detection capacity of the EIC enables the realization of of this scenario. If the GeV-scale photon were not measured, we would lose sensitivity to scalar particle emission. Since we are measuring the emitted ISR photon, the limits imposed by knowing the photon energy provides an upper bound for the energy carried by the scalar, with an integration over the probabilities of all lower ones, but this provides an exact bound on the energy (and then directly on the mass if the scalar is at rest).

A. SM DIS with ISR

As shown in [31], photon production in a factorized process at leading order can be expressed in terms of the leading order partonic cross section (without photon production) convoluted with the corresponding distribution (or fragmentation) function where the detected photon's energy is used as a cutoff for the radiative phase space. In the case of initial state leptonic radiation in DIS considered here, this amounts to a change in the QED LDF convolution in Eq. (5), as a limit on ξ. Instead of $\xi_{\min}$ in Eq. (6), the minimum is found by considering the photon would have momentum $p_\gamma=(1-\xi)E_\ell$, which would correspond to

$\xi_\gamma = 1 - p_\gamma/E_\ell$, where E_ℓ is the energy of the incoming electron of momentum ℓ. Then the minimum in the LDF convolution is $\xi_{\rm ISR} = \max(\xi_\gamma, \xi_{\rm min})$, as the kinematic constraints we have noted would still need to be satisfied for this photon to be radiated from the incoming lepton. Thus,

$$E' \frac{\mathrm{d}^3\sigma^{\mathrm{RC(LO),ISR}}_{e(\ell)h(P)\to e(\ell')\gamma X}}{\mathrm{d}^3\ell'} \approx \frac{1}{2s}\int_{\zeta_{\rm min}}^1 \frac{\mathrm{d}\zeta}{\zeta^2} D_{e/e}(\zeta,\mu^2) \int_{\xi_{\rm ISR}}^1 \frac{\mathrm{d}\xi}{\xi} f_{e/e}(\xi,\mu^2) \times \sum_q \int_{x_{\rm min}}^1 \frac{\mathrm{d}x}{x} f_{q/h}(x,\mu^2) \widehat{H}^{(2,0)}_{eq\to eX}(\hat{s},\hat{t},\hat{u}), \tag{17}$$

where $\widehat{H}^{(2,0)}_{eq\to eX}(\hat{s},\hat{t},\hat{u})$ is determined by tree-level electron-quark scattering

$$\widehat{H}^{(2,0)}_{eq\to eX} = \frac{\alpha_{\rm EM}^2 2^{2\epsilon+2}\pi^\epsilon e_Q^2 (v^2 + (v-1)^2(-\epsilon)+1)}{\hat{s}v(v-1)^2\Gamma(1-\epsilon)} \times \left(\frac{1}{\hat{s}(1-v)v}\right)^\epsilon \delta(1-w), \tag{18}$$

which is equivalent to the previously published result, though the ϵ dependence has been left explicit) [6,7]. Note that the dimensionless ratios

$$v = 1 + \frac{\hat{t}}{\hat{s}}, \qquad w = \frac{-\hat{u}}{\hat{s}+\hat{t}} \tag{19}$$

are used to simplify the expression. The LDFs and LFFs in Eq. (17) are modeled using either the perturbative model as calculated above in Sec. II or using the nonperturbative model discussed below in Sec. V. In this work, the LDF and LFF are taken to NLO, so for example, $f_{e/e}(\xi,\mu^2) = f^{(0)}_{e/e}(\xi,\mu^2) + f^{(1)}_{e/e}(\xi,\mu^2)$. However, the product of both the NLO LDF and LFF, $f^{(1)}_{e/e}(\xi,\mu^2)D^{(1)}_{e/e}(\xi,\mu^2)$, is dropped as it is suppressed by an additional power of $\alpha_{\rm EM}$.

To evaluate the total section we recall that

$$\frac{\mathrm{d}^3\ell'}{E'} = -\frac{1}{2}\mathrm{d}y\mathrm{d}Q^2\mathrm{d}\phi = \frac{Q^2}{2x_B}\mathrm{d}x_B\mathrm{d}y\mathrm{d}\phi, \tag{20}$$

where ϕ is the angle between the plane defined by the incoming and outgoing lepton momenta and the plane defined by the hadron's spin and momentum [6]. Since we consider an unpolarized process, the integral over the angular dependence $d\phi$ simply gives an overall factor of 2π, implying that the cross section can be expressed as a differential of the usual, experimentally measured kinematic variables.

The DIS with ISR process we discuss can be measured at the upcoming EIC. In the planned detector arrangement, the forward direction is taken to be in the direction of the hadron beam [27], which is opposite to the standard convention that we have also employed in this paper. In order to ensure the detected photon comes from the initial-state lepton, it must be detected in the (now) backward region, along the path of the noninteracting electrons, as the LDF is dominated by collinear emission of the radiation. This also ensures the photon does not come from the quark or hadron, as backward emission *from the hadron* is kinematically unfavorable. The ability to distinguish between the sources of the photon radiation is a vital advantage to performing an experiment like this at the EIC, as their current plans include far detectors to observe exactly such radiation [27].

B. Inclusion of a scalar

Within this context it is important to understand how the signatures of BSM physics could be observed. In this paper we present a new technique of detecting the energy loss from BSM particle emission. It is not a "bump hunt" at the resonant mass of the invisible particle, nor a displaced-vertex search, but, rather, a direct shift to the shape of the cross section as a result of the different functions included in the LDF. The diagrams for the combined radiation are shown in Fig. 3, however, the leading order contribution $f^{(0)}$ for each particle contributes as well. The perturbative LDF for the cross section calculation in Eq. (17) is modified by including the scalar LDF as calculated for a generic spin 0 particle in Sec. III, and the factorized DIS cross section of Eq. (5) is also modified. Here we replace the integral over the LDF in Eq. (5) as follows

$$\begin{aligned}
&\int_{\xi_{\rm ISR}}^1 \frac{\mathrm{d}\xi}{\xi} f_{e/e}(\xi,\mu^2) \\
&\Rightarrow \int_{\xi_{\rm ISR}}^1 \frac{\mathrm{d}\xi}{\xi} f^{\rm QED}_{e/e}(\xi,\mu^2) \int_{\xi'_{\rm ISR}}^1 \frac{\mathrm{d}\xi'}{\xi'} f^{\rm s}_{e/e}(\xi',\mu^2) \\
&\approx \int_{\xi_{\rm ISR}}^1 \frac{\mathrm{d}\xi}{\xi} f^{(0),\rm QED}_{e/e}(\xi,\mu^2) \int_{\xi_{\rm min}}^1 \frac{\mathrm{d}\xi'}{\xi'} f^{(0),\rm s}_{e/e}(\xi',\mu^2) \\
&\quad + \int_{\xi_{\rm ISR}}^1 \frac{\mathrm{d}\xi}{\xi} f^{(1),\rm QED}_{e/e}(\xi,\mu^2) \int_{\xi_{\rm min}}^1 \frac{\mathrm{d}\xi'}{\xi'} f^{(0),\rm s}_{e/e}(\xi',\mu^2) \\
&\quad + \int_{\xi_{\rm ISR}}^1 \frac{\mathrm{d}\xi}{\xi} f^{(0),\rm QED}_{e/e}(\xi,\mu^2) \int_{\xi_{\rm min}}^1 \frac{\mathrm{d}\xi'}{\xi'} f^{(1),\rm s}_{e/e}(\xi',\mu^2) \\
&\quad + \int_{\xi_{\rm ISR,1}}^1 \frac{\mathrm{d}\xi}{\xi} f^{(1),\rm QED}_{e/e}(\xi,\mu^2) \int_{\xi_{\rm ISR,2}}^1 \frac{\mathrm{d}\xi'}{\xi'} f^{(1),\rm s}_{e/e}(\xi',\mu^2) \\
&\quad + \int_{\xi'_{\rm ISR,1}}^1 \frac{\mathrm{d}\xi'}{\xi'} f^{(1),\rm s}_{e/e}(\xi',\mu^2) \int_{\xi'_{\rm ISR,2}}^1 \frac{\mathrm{d}\xi}{\xi} f^{(1),\rm QED}_{e/e}(\xi,\mu^2),
\end{aligned} \tag{21}$$

where in the limits of integration shown we have specialized to the ISR case as per our discussion in Sec. IV A. Here ξ' is the momentum fraction carried by the electron after the

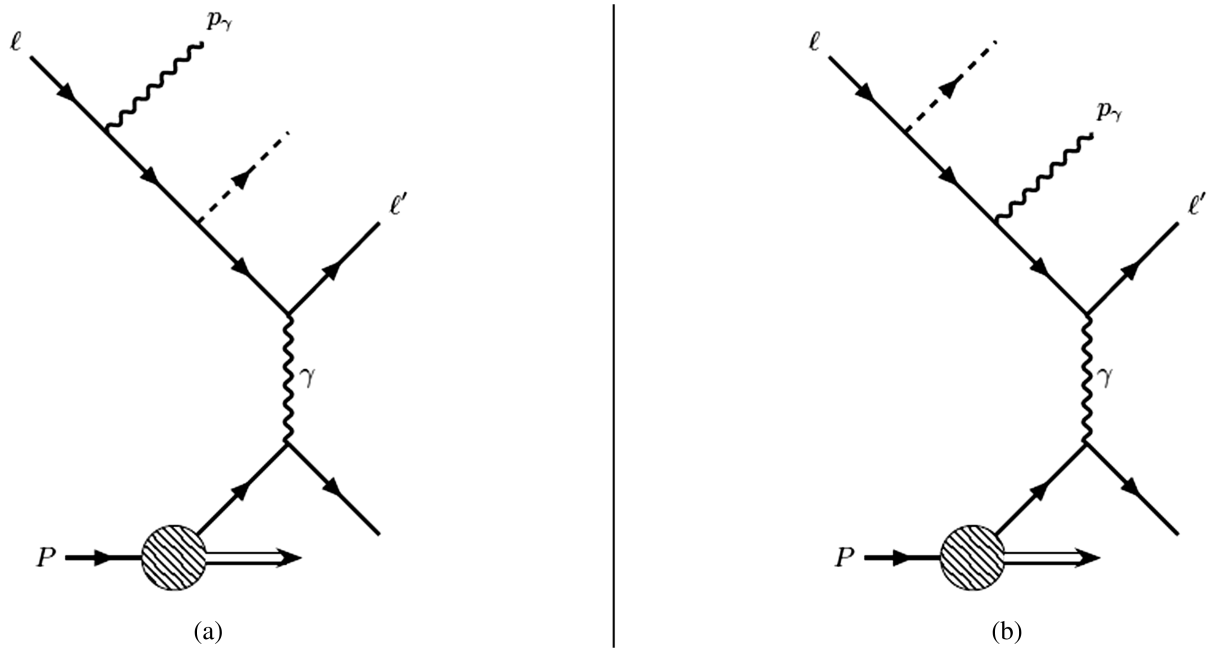


FIG. 3. Feynman diagrams for DIS with combined QED and scalar ISR, with the scenario of the photon radiation occurring first in (a) or the scalar radiation occurring first in (b).

emission of the scalar, and it is integrated through a convolution similar to that in ξ. If both LDF contributions are taken in NLO, the order of the emission affects the kinematic limits, and its numerical subscript, either $\xi^{(\prime)}_{\mathrm{ISR},1}$ or $\xi^{(\prime)}_{\mathrm{ISR},2}$, reflects which one is emitted first. If the photon is emitted first, $\xi_{\mathrm{ISR},1} = \max(\xi_\gamma, \xi_{\min})$ and $\xi_{\mathrm{ISR},2} = \hat{\xi}_{\min} = (1-\hat{y})\hat{s}/(\hat{s}-\hat{Q}^2)$, whereas if the scalar is emitted first, $\xi'_{\mathrm{ISR},1} = \max(1-\xi_\gamma, \xi_{\min})$ and $\xi'_{\mathrm{ISR},2} = \max(\hat{\xi}_\gamma, \hat{\xi}_{\min})$, where $\hat{\xi}_\gamma = 1 - p_\gamma/\xi' E_\ell$.

The LFF is not expanded similarly, as in this work we suppose the scalar is emitted from the initial state electron only. By taking the ratio of the DIS with ISR cross section for the various BSM physics models to the same DIS with ISR cross section for only SM behavior, significant deviations from unity can occur as a function of the kinematics. Particularly, forming similar ratios of the experimental cross section measurements and the outcomes of different models, be it the SM or various BSM scenarios, can be used as evidence for exotic physics contributions—or can be potentially ruled out if the expected deviation does not occur. This requires a precise understanding of the associated LDFs and LFFs, both within and beyond the SM. The nonperturbative LDFs and LFFs that can arise from QCD interactions from photon splitting, such as into a $q\bar{q}$ pair at nonperturbative scales, where we note [66] for further discussion, or simply from noncollinear emission effects, which can include BSM physics, should be determined from fitting the lepton functions to DIS experimental data. As shown in [66], the evolution kernels we used in Eq. (4) address the broader class of splitting functions possible under the full QED and QCD framework. When BSM physics is included, new terms appear in the evolution kernels, though such effects turn out to be negligible for the range of empirically allowed scaling couplings. We regard the nonperturbative LDFs as potentially reflective of the possibility of new physics nonetheless, because they should ultimately be fit to the experimental data—and in which the new scalar may appear. Given this setting, we advocate for new-physics probes in which the modeled nonperturbative LDF modifies the computed observable in a minimal way—but for which the changes due to the use of the perturbative LDF with scalar emission can be readily determined.

Currently, there have not been any determinations of the nonperturbative LDFs and LFFs, due to a lack of suitable lepton scattering data. This is because nearly all the existing, published lepton scattering data have already had radiative corrections applied, usually through the methods described in [9,11,13–17]. However, this unfortunate situation is slowly changing. For example, a recent analysis of ZEUS data explicitly defines the radiative correction factor [67], making it possible to reconstruct the "deradiated" (uncorrected) data. Also an effort has been completed in which the needed uncorrected data has been reconstructed from old ALEPH data [68], and upcoming world-wide experimental programs can also report their new data without radiative corrections. Under the inclusion of BSM physics, the nonperturbative model could be further modified, and indeed can offer another avenue by which to differentiate models, however adjustments to the evolution kernels alone do not indicate important effects.

V. RESULTS

A. Scalar emission model

The DIS with ISR cross section reported in Eq. (17) has been evaluated at a particular choice of EIC kinematics, specifically, $\sqrt{s} = 140$ GeV, $E_\ell = 18$ GeV, and $0.01 < y < 0.95$ [27], using CTEQ 18 unpolarized PDFs [69], and using either a perturbative expression *or* a nonperturbative model for the LDFs and LFFs. The perturbative expression is given in Eq. (21). The nonperturbative model employs the ansatz

$$f(x,\mu_0^2) = \frac{x^\alpha (1-x)^\beta}{B(\alpha+1,\beta+1)}, \tag{22}$$

where we note [70] for discussion of the quark and gluon content of the electron at high energies. Here we suppose Eq. (22) is given at an input factorization scale of $\mu_0 = m_c$, the mass of the charm quark, so that our expression must be evolved to the scale pertinent to our analysis. To do this, we use DGLAP-equivalent evolution equations for the LDF and LFF [5,6]. Since our ansatz carries no explicit μ^2 dependence, it is introduced through its evolution, using Eq. (4). In this work, (α,β) are chosen to be (5, 0.5) and (50, 0.125) to match the behavior described in [7]. In previous work, it has been shown that large corrections may arise as a result of the nonperturbative models of the LDFs and LFFs [7]. We avoid this issue in two ways. First, we will only be comparing cross sections calculated using the joint QED and QCD factorization approach, making the effect of the corrections due to the nonperturbative model smaller, because the radiative corrections appear in both the scalar and SM-only calculations. Second, we will take ratios between observables calculated at different kinematics to reduce the impact of the ansatz parametrization. These ratios will be explained further in what follows.

The kinematic limits for p_γ and Q^2 are

$$Q^2_{\max} = \frac{s(E_\ell y - p_\gamma)}{E_\ell - p_\gamma}$$
$$p_{\gamma,\max} = E_\ell \left(\frac{sy-1}{s-1}\right). \tag{23}$$

The limits are found by enforcing $\xi_{\min} < \xi < 1$, where the minimum comes from Eq. (6) with $\zeta = 1$, and $Q^2 > 1$. The relation to y is shown in Fig. 4, where the vertical dashed lines show the choices for y used when comparing kinematic regions. A p_γ minimum of $0.6 p_{\gamma,\max}$ is used to focus on the region where the perturbative and nonperturbative LDF (or LFF) show reasonable agreement, before additional modifications were studied, in order to minimize the differences resulting from the two descriptions. This limit also ensures the observed photon is hard for the process. The $Q^2_{\max}$ relationship is shown in Fig. 5, again with the minimum p_γ cut we have noted.

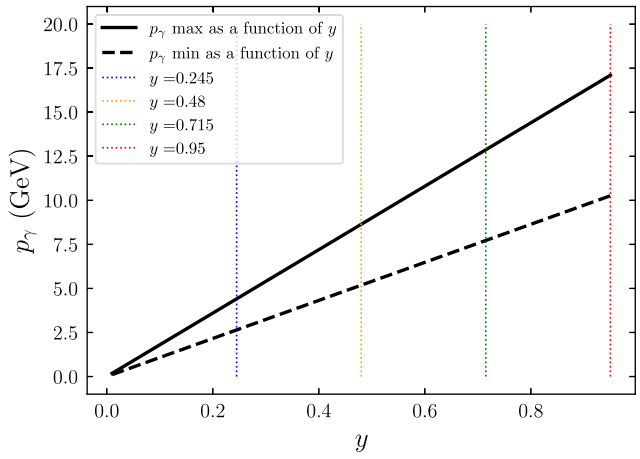


FIG. 4. The variables $p_{\gamma,\max}$ and $p_{\gamma,\min}$ as a function of y at specific EIC kinematics ($\sqrt{s} = 140$ GeV and $E_\ell = 18$ GeV).

The specific kinematics within the EIC range are chosen to maximize the effects of the radiative corrections. As shown in [14], the high y region has the most impact from radiative corrections, as the corrections to the cross section can be of the same order of magnitude as the cross section itself. The work in [5–7] extend this demonstration to the QED and QCD joint factorization method and similarly show the same kinematic region has a high impact from the LDF and LFF. By construction, the high p_γ region implies a large shift from the effect of radiative corrections.

The mass and coupling choices for the scalar emission have been made with [26] in mind. We explore the mass range from 10^{-5} GeV to 1 GeV, where the upper limit is constrained by the kinematics of the photon and scalar

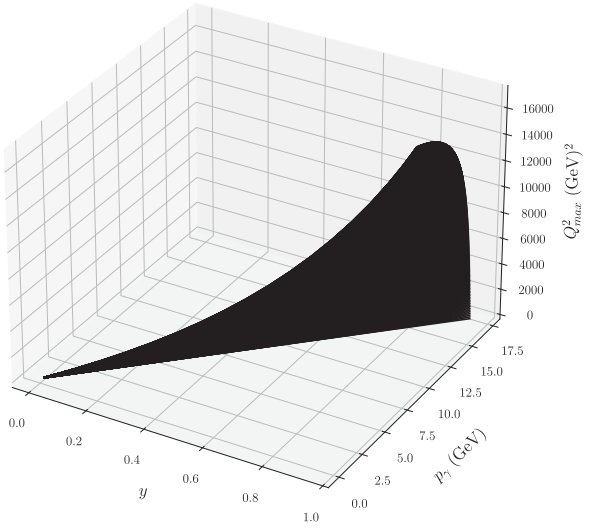


FIG. 5. Kinematically allowable region for $Q^2_{\max}$ in terms of p_γ and y at specific EIC kinematics ($\sqrt{s} = 140$ GeV and $E_\ell = 18$ GeV).

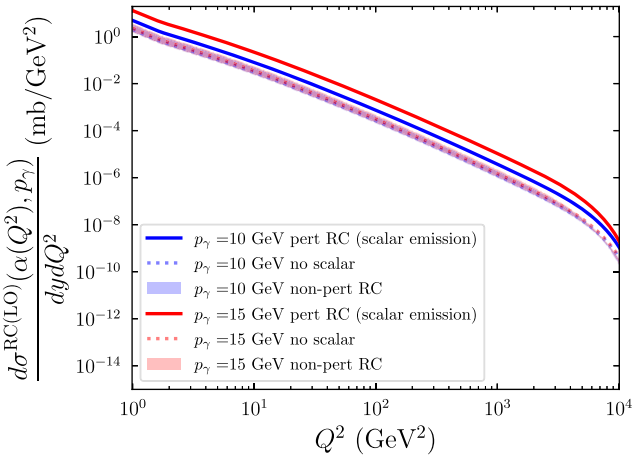


FIG. 6. Cross section comparison for $m_S = 0.9$ GeV and $g_{se} = 3 \times 10^{-6}$ at specific EIC kinematics ($\sqrt{s} = 140$ GeV, $E_\ell = 18$ GeV, and $y = 0.95$).

emission case, as the energy of the scalar must be less than the energy of the incoming lepton beam minus the energy of the radiated photon, and the remaining energy after both emissions must be large enough to factorize DIS (i.e., $Q^2 > 1$ GeV^2). The coupling range explored was $10^{-9} \leq g_{se} \leq 10^{-2}$, which covers the range in [26] for leptophilic scalars. All the observables considered below use $y = 0.95$, as this is the region with the largest possible radiative effects, but also with the sharpest limit on possible scalar mass, which emerges from allowing the largest possible p_γ. We also use the conventional choice of $\mu^2 = Q^2$; however, we tested other choices for μ^2, such as $\mu^2 = p_\gamma^2$, and found no effects on the results. However, for low y, p_γ is not a reasonable choice for the factorization scale, as it becomes too small, i.e., $p_\gamma^2 < 10$ GeV^2, thus potentially limiting the validity of the factorization approximation.

B. Observables

Various DIS with ISR cross sections are shown in Fig. 6. We show the cross sections for DIS with ISR, that is, with an observed photon with energy p_γ and unobserved scalar radiation, as well as DIS with ISR without any scalar emission. In what follows we consider various cross section ratios in order to display the effects of interest more clearly. Our use of ratios should also reduce the sensitivity of our predictions to the order of perturbation theory in which we work. As a first example, we consider

$$\hat{\mathcal{O}}_1 = \frac{\sigma^{\mathrm{DIS,ISR}(p_\gamma),s}}{\sigma^{\mathrm{DIS,ISR}(p_\gamma)}}, \tag{24}$$

where

$$\sigma^{\mathrm{DIS,ISR}(p_\gamma),s} = \frac{\mathrm{d}^2\sigma^{\mathrm{RC(LO),ISR,s}}(\alpha(Q^2), p_\gamma, y)}{\mathrm{d}y\mathrm{d}Q^2},$$
$$\sigma^{\mathrm{DIS,ISR}(p_\gamma)} = \frac{\mathrm{d}^2\sigma^{\mathrm{RC(LO),ISR}}(\alpha(Q^2), p_\gamma, y)}{\mathrm{d}y\mathrm{d}Q^2}.$$

This ratio, $\hat{\mathcal{O}}_1$ or observable 1, is shown in Fig. 7, and we see that the effects of the scalar emission can reach over five times the QED-only cross section. In all cases we have used the SM cross section computed with the perturbative LDF in the denominator and have included the running of $\alpha_{\mathrm{EM}}(Q^2)$. Here we use the nonperturbative LDF shown in Eq. (22) as a proxy for the additional possibility of non-SM effects, such as the scalar emission model we assume here, in that soft function. The bands from the nonperturbative ansatz for the LDF appear to be well-separated from that of the perturbative LDF cases, but they nevertheless suggest the need to extract those LDFs precisely to ensure that they do not introduce more uncertainty, which appears to be more impactful in lower kinematic regions, such as in y or Q^2.

Our analysis exists in advance of suitable experimental data. In the future, the EIC data, e.g., can be used to replace either model in the calculation of the ratios. If the data is assumed to follow the SM, then it can serve as the QED-only model in these ratios, and deviations from the SM could very well appear differently than in our plots, possibly yielding a ratio of approximately unity if it follows the BSM model we have noted. If, rather, we assume the data follow our scalar emission model, then the comparison should appear closer to our plots here, as our results show the deviations from the leading QED-only radiation, which is the dominant SM contribution.

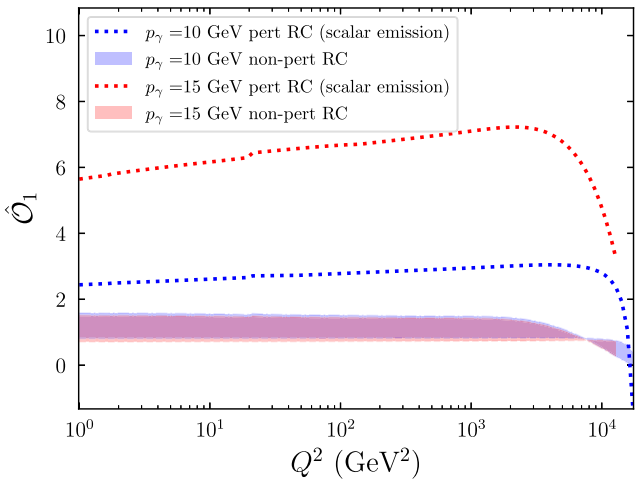


FIG. 7. Observable 1 for $m_S = 0.9$ GeV and $g_{se} = 3 \times 10^{-6}$ at specific EIC kinematics ($\sqrt{s} = 140$ GeV, $E_\ell = 18$ GeV, and $y = 0.95$).

There are further ratios we can consider. We can consider the ratio of the DIS with ISR cross sections, with or without the unobserved scalar radiation, evaluated in two different kinematic regions. In that case, one region can be chosen so that it is less kinematically favorable to strong ISR. Thus the effects of the radiation can be observed also, and we provide examples in what follows. Namely, we consider ratios computed at the different values of y, as in the ratio $\hat{\mathcal{O}}_2$, observable 2, given by

$$\hat{\mathcal{O}}_2 = \frac{\sigma_{y2}}{\sigma_{y1}}, \tag{25}$$

with either

$$\sigma_{y2} = \frac{\mathrm{d}^2\sigma^{\mathrm{RC(LO),ISR,s}}(\alpha(Q^2), p_\gamma, y_2)}{\mathrm{d}y\mathrm{d}Q^2}$$
$$\sigma_{y1} = \frac{\mathrm{d}^2\sigma^{\mathrm{RC(LO),ISR,s}}(\alpha(Q^2), p_\gamma, y_1)}{\mathrm{d}y\mathrm{d}Q^2} \tag{26}$$

or

$$\sigma_{y2} = \frac{\mathrm{d}^2\sigma^{\mathrm{RC(LO),ISR}}(\alpha(Q^2), p_\gamma, y_2)}{\mathrm{d}y\mathrm{d}Q^2}$$
$$\sigma_{y1} = \frac{\mathrm{d}^2\sigma^{\mathrm{RC(LO),ISR}}(\alpha(Q^2), p_\gamma, y_1)}{\mathrm{d}y\mathrm{d}Q^2}, \tag{27}$$

or of p_γ, as in the ratio $\hat{\mathcal{O}}_3$, observable 3, given by

$$\hat{\mathcal{O}}_3 = \frac{\sigma_{p_{\gamma,2}}}{\sigma_{p_{\gamma,1}}}, \tag{28}$$

with either

$$\sigma_{p_{\gamma,2}} = \frac{\mathrm{d}^2\sigma^{\mathrm{RC(LO),ISR,s}}(\alpha(Q^2), p_{\gamma,2}, y)}{\mathrm{d}y\mathrm{d}Q^2}$$
$$\sigma_{p_{\gamma,1}} = \frac{\mathrm{d}^2\sigma^{\mathrm{RC(LO),ISR,s}}(\alpha(Q^2), p_{\gamma,1}, y)}{\mathrm{d}y\mathrm{d}Q^2} \tag{29}$$

or

$$\sigma_{p_{\gamma,2}} = \frac{\mathrm{d}^2\sigma^{\mathrm{RC(LO),ISR}}(\alpha(Q^2), p_{\gamma,2}, y)}{\mathrm{d}y\mathrm{d}Q^2}$$
$$\sigma_{p_{\gamma,1}} = \frac{\mathrm{d}^2\sigma^{\mathrm{RC(LO),ISR}}(\alpha(Q^2), p_{\gamma,1}, y)}{\mathrm{d}y\mathrm{d}Q^2}. \tag{30}$$

These observables have been considered for the perturbative and nonperturbative models for the LDFs and LFFs separately. In the first case [observable 2, Eq. (25)], two different choices for y are used, and the p_γ range is taken to match the more restrictive kinematics of the lower y value, as shown in Fig. 8. This restriction on the p_γ range severely limits the observable effects of the scalar radiation, indicating that this ratio is not useful in searching for signs of exotic particle emission.

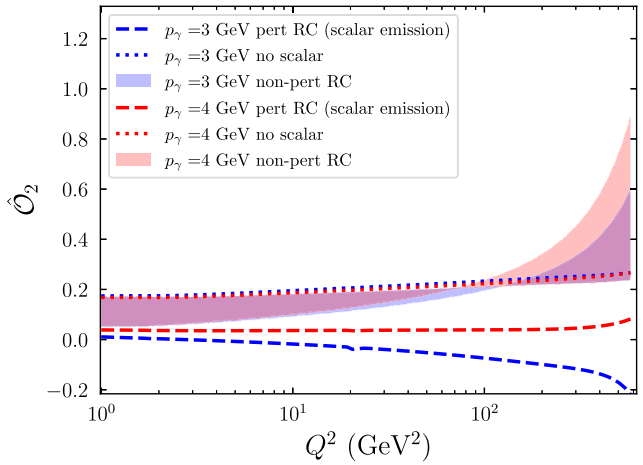


FIG. 8. Observable 2 for $m_S = 0.9$ GeV and $g_{se} = 3 \times 10^{-6}$ at specific EIC kinematics ($\sqrt{s} = 140$ GeV, $E_\ell = 18$ GeV, and with $y_1 = 0.24$ and $y_2 = 0.95$).

Turning to observable 3, Eq. (28), where a fixed y value but different p_γ values are chosen, as illustrated in Fig. 9, we see the shift due to the possible scalar emission with a more energetic photon is highly emphasized compared to the lower energy photon emission, with a clear separation between the scalar emission model and QED-only DIS with ISR. The nonperturbative model results are also suppressed in this ratio comparison, as seen by the highlighted bands lying close to the bottom of the plot, near a ratio value of 1.

Finally, we consider "super ratios" of the $\hat{\mathcal{O}}_2$ and $\hat{\mathcal{O}}_3$ observables we have considered thus far. That is, we have $\hat{\mathcal{O}}_4$, observable 4,

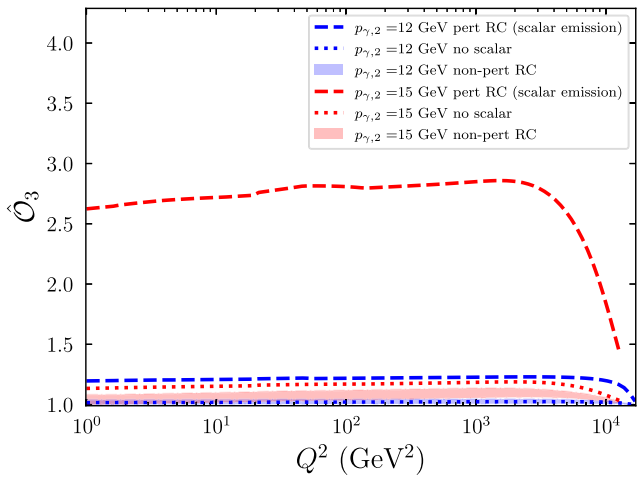


FIG. 9. Observable 3 for $p_{\gamma,1} = 10$ GeV, $m_S = 0.9$ GeV, and $g_{se} = 3 \times 10^{-6}$ at specific EIC kinematics ($\sqrt{s} = 140$ GeV, $E_\ell = 18$ GeV, and $y = 0.95$).

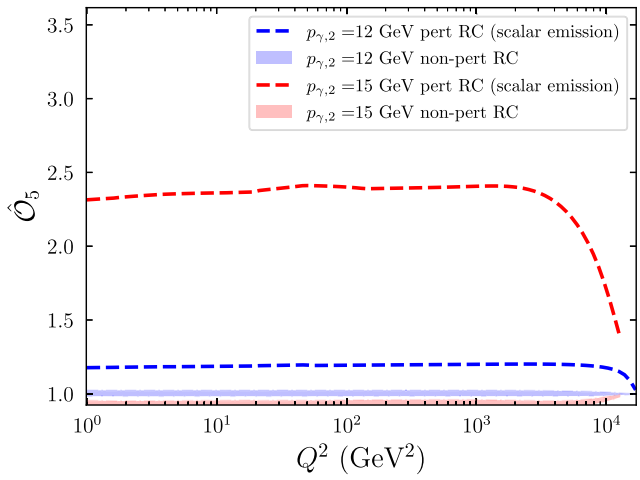


FIG. 10. Observable 5 for $p_{\gamma,1} = 10$ GeV, $m_S = 0.9$ GeV and $g_{se} = 3 \times 10^{-6}$ at specific EIC kinematics ($\sqrt{s} = 140$ GeV, $E_\ell = 18$ GeV, and $y = 0.95$).

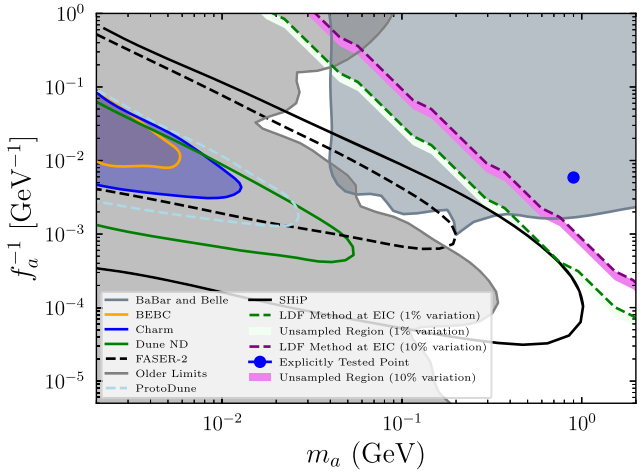


FIG. 11. A facsimile of the left panel of Fig. 9 in [26], where we note $f_a^{-1} = g_{se}/m_e$, since our methods do not distinguish a scalar from an axion, along with the sensitivity limits from the current work for the kinematics of $y = 0.95$, $Q^2 = 0.75Q^2_{\max}$, and $p_\gamma = 0.9p_{\gamma,\max}$. Our "LDF method" results show by how much the computed BSM cross sections can differ from the SM ones in the noted kinematic region, through their ratios, with the associated soft bands indicating the possible variation due to the limited resolution in the sampling of the BSM model parameter space. The single blue point indicates the mass and coupling used in the studies of Figs. 6–10. The compilation of Ema *et al.* [26] shows excluded regions on the parameter space from existing experiments as shaded regions (typically at 90% CL), and the solid and dashed lines are forecasts. In all cases, these collected results and forecasts limit a produced scalar ϕ through nonobservation of $\phi \to e^+e^-$. The sensitivity limits we show also constrain models in which ϕ could decay to other dark-sector particles, rendering them distinct from all the others shown. We refer to the text for all details.

$$\hat{\mathcal{O}}_4 = \frac{\hat{\mathcal{O}}_{2,\text{Scalar}}}{\hat{\mathcal{O}}_{2,\text{QED Only}}} = \frac{\hat{\mathcal{O}}_1(y_2)}{\hat{\mathcal{O}}_1(y_1)} \tag{31}$$

and $\hat{\mathcal{O}}_5$, observable 5,

$$\hat{\mathcal{O}}_5 = \frac{\hat{\mathcal{O}}_{3,\text{Scalar}}}{\hat{\mathcal{O}}_{3,\text{QED Only}}} = \frac{\hat{\mathcal{O}}_1(p_{\gamma,2})}{\hat{\mathcal{O}}_1(p_{\gamma,1})}. \tag{32}$$

Observable 4, the super ratio in y, is not a useful discriminant, so that it is not shown, but observable 5 is a much more effective one, in that it completely minimizes the effects of the nonperturbative LDF and can help identify the scalar behavior. This is shown in Fig. 10, where the nonperturbative effects are barely visible along the Q^2 axis.

Overall, since our limits apply to axionlike particles as well, we can compare to the analysis of limits on MeV-GeV scale axions from Ema *et al.* [26]. Those authors consider limits on axion-lepton coupling in various flavorful scenarios. In that case it turns out that the couplings in the μ-phobic axion scenario, with $g_{a\mu} = 0$ and $g_{ae} = g_{a\tau} = m_e/f_a$, where f_a is a parameter to be determined, are the most poorly constrained. This is shown in the left panel of their Fig. 9 [26], which is roughly reproduced for a proof-of-principle comparison in Fig. 11. Our examples in Figs. 6–10 employ $g_{se} = 3 \times 10^{-6}$ or $f_a^{-1} = 6 \times 10^{-3}$ GeV^{-1} and a scalar mass of 0.9 GeV, which is indicated as a single blue point. If we set aside the possibility of dark decays of the scalar, this lies above the border of the parameter space excluded by the *BABAR* [71] and Belle [72] data. Even so, these examples are illustrative of the effect a scalar candidate would have on the cross section, and sample data point calculations for $g_{se} \approx 3 \times 10^{-7}$, or $f_a^{-1} \approx 6 \times 10^{-4}$, show the trends would be similar, but slightly smaller in magnitude. This choice for g_{se} around 10^{-7} falls outside the excluded region while remaining within the sensitivity limits from this study. The reasoning for the original parameter choice is explained in the Appendix.

Here we work in the kinematics of $y = 0.95$, $Q^2 = 0.75Q^2_{\max}$, and $p_\gamma = 0.9p_{\gamma,\max}$ to focus on a region with the largest effects. For this case, the limits from this study, a general spin 0 leptophilic candidate, are added in dashed green and purple. These represent changes at the level of 1% or 10% in the cross section ratio $\hat{\mathcal{O}}_1$, respectively, meaning that the cross section with scalar emission changes by at least that amount from the SM-only cross section. In contrast to the limits and forecasts in Ema *et al.* [26], the dashed lines from this study represent a deviation from a cross section ratio of unity across a smooth region. The variations chosen for this plot are simply illustrative of the parameter space this method can probe, and any expected deviation from the SM-only prediction can be used to point to a discovery. The lighter bands represent the range of possible testable candidates which could fall in the given variation level, as the given limits

were found by dividing the mass and coupling phase space into 50 points each. The cross section ratio was calculated at each pair for the given kinematics, and the deviation was checked to be at least the desired size. Thus, there would be some mass and coupling points that fall between the chosen ones, and the band thickness follow from determining where the tested parameter choice was found to have insufficient deviation from the SM-only prediction. When considering the expected integrated luminosity of the EIC to be ≈ 10 fb^{-1} per year [27], the number of events expected is estimated to be roughly 10^9, provides a comfortable margin for detector limitations, i.e., imperfect detector efficiency, to ensure strong statistics.

VI. SUMMARY AND OUTLOOK

In this paper we have set out a new search strategy at accelerators for the emission of non-SM particles of varying mass and spin through the detection of anomalous energy loss, i.e., through the determination of the modification of the cross section that their emission would generate. This new strategy is made possible through the use of the joint QED and QCD factorization of deeply inelastic, electron-proton scattering [5–7], because it provides a systematic treatment of the radiative corrections that appear. This approach eliminates the parameter-dependent corrections that can vary from framework to framework in earlier work, at the price of introducing universal, nonperturbative LDF and LFF functions to be determined from DIS experiments. Here we have leveraged the sensitivity of the resulting cross section to new, light, weakly coupled particle emission through the additional requirement of detecting an energetic photon from ISR. In this paper we have studied the particular case of spin 0 particle emission, because our approach, at its current level of refinement, does not determine the parity of that emitted, energetic particle, to show that in the case of an EIC study we can expect to probe previously unconstrained BSM parameter space, particularly at MeV-GeV scales, concretely.

We expect the forthcoming EIC to give us new insight into the physics of the femtometer scale. At this new frontier we can probe not only the intricate color, spin, and flavor correlations of the strongly interacting quarks and gluons within nucleons [73], but we also see that it opens the possibility of studying non-SM physics in the challenging MeV-GeV regime of new particle masses, for which other sorts of experiments are under development worldwide [25,74–76].

The possibility of displaced vertex searches have already been discussed for study at the EIC [77,78], and we would like to emphasize that the anomalous energy loss search we advocate allows us to probe a broader class of models. The displaced vertex search for a new scalar, say, has a sensitivity that scales as g_{se}^4, and it requires that the new particle materializes into a dilepton pair. However, in an analogous anomalous energy loss search (here our LDF method), which scales as g_{se}^2, the new particle can decay to other, unspecified, particles of the hidden sector. When the coupling to other dark-sector particles is larger than the SM coupling, these other decay modes are more likely, making it harder to detect the decay of the new particle into a dilepton pair in a displaced vertex search. In this manner the anomalous energy loss method probes a much broader class of models and opens access to weaker g_{se} couplings as well.

Although we have focused on probing the possibility of spin 0 particle emission, many sorts of particle probes and tests are possible. We have noted these broader prospects throughout the paper, and we have enumerated the quantum numbers and certain interactions of the dark matter particles accessible to us in Table I. Here, in summary, we collect some of the possibilities in an organized way. We believe the MeV-GeV mass scale opens a number of interesting questions to explore, even if the various BSM particle candidates could appear with an enormous range of masses. Particularly,

(i) We have discussed how the comparison of dimension 4 and 5 spin 0 particle-electron interactions are sensitive to the parity of the spin 0 particle. In particular, in the axionlike case, the possibility of the process $\gamma^* \to a\gamma$, radiated from an electron line, would seem to be required to connect the two descriptions precisely. This process, in turn, feeds into the nonperturbative LDF, thus yielding a BSM contribution to its construction, and showing that this object can be different in the SM and BSM cases.

(ii) We observe that our current RC(LO) analysis would only allow us to fit for nonperturbative SM and BSM LDFs separately through differences in their respective splitting functions. However, if we were to extend our analysis to NLO in the hard part, the BSM particle would appear explicitly and thus provide additional distinguishing features for that analysis.

(iii) Although we have focused on other possibilities in this paper, it should also be possible to study massive spin 2 particles with our methods as well, albeit they are typically considered in mass regions apropos to ultralight dark matter, i.e., at sub-eV scales.

(iv) The joint QED and QCD factorization framework allows us to step beyond the cross section to probe the interactions of the partons in the struck hadron in an DIS event. Particularly, we think that the study of the energy-energy correlators in this context could prove a powerful way of probing the possibility of energy loss from hidden-sector interactions with gluons.

We look forward to future exploration of these issues and more at the EIC and elsewhere.

ACKNOWLEDGMENTS

We gratefully acknowledge discussions with Jianwei Qiu, particularly of his work on isolated photon emission in DIS [31], that we utilize here, and we also thank the U.S. Department of Energy, Office of Nuclear Physics, under Grants No. DE-FG02-96ER40989 and DE-FG02-99ER41101 for partial support. We would like to acknowledge Hooman Davoudiasl for a helpful comment. We thank the BNL EIC Theory institute for their hospitality while this paper is in preparation. This work has been partially funded by the Deutsche Forschungsgemeinschaft (DFG, German Research Foundation) No. 491245950.

DATA AVAILABILITY

There are no publicly available research data or software supporting this manuscript. Requests for further information or data should be sent to the authors.

APPENDIX: DETAILED KINEMATIC CHOICES

The exact kinematic inputs were found by setting the bounds for the range of each value and dividing it into even segments. The results above show the rounded, "clean" numbers for reference, however, here the exact values will be listed. For the range of y, it was taken as the expected EIC values, 0.01 to 0.95, then divided into five segments (including the end points), so for the ratio between y_1 and y_2, the y_1 is 0.245 exactly (all the exact y values are shown in Fig. 4). The mass of the scalar was evenly distributed over a logarithmic space (also with 5 segments), from 10^{-5} GeV to the max allowed m_S for a given kinematic $(E_\ell - p_\gamma)$, meaning the larger y limited the p_γ and therefore the m_S, so for $y = 0.95$, the largest m_S possible was 9.0005×10^{-1} GeV, which was reported above at the tenth of a GeV level. Similarly, the g_{se} range was evenly distributed over five segments of a logarithmic space from 10^{-9} to 10^{-2}, which made the exact value for coupling above to be $g_{se} = 3.162 \times 10^{-6}$. The p_γ range was divided into five segments also, but linearly over the range from the imposed minimum of $0.6 p_{\gamma,\max}$ to $0.9 p_{\gamma,\max}$. The minimum cutoff is discussed above, but the maximum cutoff was chosen to avoid end point issues as when $p_\gamma = p_{\gamma,\max}$, $Q^2_{\max} = 1$, which severely limits the viability of factorization at this scale [see Eq. (23)]. The exact values for each the p_γ above are then (all in units of GeV): $15 \to 15.39$, $12 \to 11.54$, $10 \to 10.26$, $4 \to 3.97$, and $3 \to 2.65$, where we left the values at the two decimal places for simplicity. These more precise values are included here to ensure reproducibility of our results with the same kinematic choices.

[1] A. S. Chou *et al.*, in Snowmass 2021 (2022), arXiv:2211.09978.
[2] R. Alarcon *et al.*, in Snowmass 2021 (2022), arXiv:2203.08103.
[3] B. P. Abbott *et al.*, Phys. Rev. X **6**, 041015 (2016).
[4] C. de Rham, Living Rev. Relativity **17**, 7 (2014).
[5] T. Liu, W. Melnitchouk, J.-W. Qiu, and N. Sato, Phys. Rev. D **104**, 094033 (2021).
[6] T. Liu, W. Melnitchouk, J.-W. Qiu, and N. Sato, J. High Energy Phys. 11 (2021) 157.
[7] J. Cammarota, J.-W. Qiu, K. Watanabe, and J.-Y. Zhang, Phys. Rev. D **112**, 056007 (2025).
[8] Y.-S. Tsai, Phys. Rev. **122**, 1898 (1961).
[9] L. W. Mo and Y. S. Tsai, Rev. Mod. Phys. **41**, 205 (1969).
[10] Y.-S. Tsai, in *Proceedings of NATO Advanced Institute on Electron Scattering and Nuclear Structure, Cagliari* (1971).
[11] D. Y. Bardin and N. M. Shumeiko, Nucl. Phys. **B127**, 242 (1977).
[12] D. Y. Bardin, C. Burdik, P. C. Khristova, and T. Riemann, Z. Phys. C **42**, 679 (1989).
[13] D. Y. Bardin, K. C. Burdik, P. K. Khristova, and T. Riemann, Z. Phys. C **44**, 149 (1989).
[14] B. Badelek, D. Y. Bardin, K. Kurek, and C. Scholz, Z. Phys. C **66**, 591 (1995).
[15] J. Kripfganz, H. J. Mohring, and H. Spiesberger, Z. Phys. C **49**, 501 (1991).
[16] H. Spiesberger, Phys. Rev. D **52**, 4936 (1995).
[17] J. Blumlein and H. Kawamura, Eur. Phys. J. C **51**, 317 (2007).
[18] A. Patella, Proc. Sci. LATTICE2016 (**2017**) 020. [arXiv:1702.03857].
[19] H.-W. Lin, Prog. Part. Nucl. Phys. **144**, 104177 (2025).
[20] L. Cieri, G. Ferrera, and G. F. R. Sborlini, J. High Energy Phys. 08 (2018) 165.
[21] A. Autieri, L. Cieri, G. Ferrera, and G. F. R. Sborlini, J. High Energy Phys. 07 (2023) 104.
[22] L. Buonocore, L. Rottoli, and P. Torrielli, J. High Energy Phys. 07 (2024) 193.
[23] A. Autieri, S. Camarda, L. Cieri, G. Ferrera, and G. Sborlini, J. High Energy Phys. 03 (2026) 113.
[24] D. de Florian and L. P. Conte, Eur. Phys. J. C **86**, 118 (2026).
[25] A. Berlin, N. Blinov, G. Krnjaic, P. Schuster, and N. Toro, Phys. Rev. D **99**, 075001 (2019).
[26] Y. Ema, P. J. Fox, M. Hostert, T. Menzo, M. Pospelov, A. Ray, and J. Zupan, Phys. Rev. D **112**, 115028 (2025).
[27] R. Abdul Khalek *et al.*, Nucl. Phys. **A1026**, 122447 (2022).
[28] I. Moult and H. X. Zhu, arXiv:2506.09119.

[29] Y. Guo, W. Vogelsang, F. Yuan, and W. Zhao, Phys. Rev. D **113**, 074027 (2026).
[30] A. Anastasi *et al.*, Phys. Lett. B **767**, 485 (2017).
[31] E. L. Berger and J. Qiu, Phys. Lett. B **248**, 371 (1990).
[32] S. Weinberg, Phys. Rev. **135**, B1049 (1964).
[33] M. Fierz and W. Pauli, Proc. R. Soc. A **173**, 211 (1939).
[34] M. Maggiore, *Gravitational Waves: Volume 1: Theory and Experiments* (Oxford University Press, New York, 2007).
[35] J. C. Collins, D. E. Soper, and G. F. Sterman, Nucl. Phys. **B261**, 104 (1985).
[36] J. C. Collins and D. E. Soper, Nucl. Phys. **B194**, 445 (1982).
[37] J. Collins, *Foundations of Perturbative QCD* (Cambridge University Press, Cambridge, England, 2011), Vol. 32.
[38] J. B. Kogut and D. E. Soper, Phys. Rev. D **1**, 2901 (1970).
[39] G. P. Lepage and S. J. Brodsky, Phys. Rev. D **22**, 2157 (1980).
[40] G. Altarelli and G. Parisi, Nucl. Phys. **B126**, 298 (1977).
[41] V. N. Gribov and L. N. Lipatov, Sov. J. Nucl. Phys. **15**, 438 (1972).
[42] D. de Florian, G. F. R. Sborlini, and G. Rodrigo, Eur. Phys. J. C **76**, 282 (2016).
[43] D. de Florian, G. F. R. Sborlini, and G. Rodrigo, J. High Energy Phys. 10 (2016) 056.
[44] V. Silveira and A. Zee, Phys. Lett. **161B**, 136 (1985).
[45] D. J. E. Marsh, Phys. Rep. **643**, 1 (2016).
[46] J. M. Cline, K. Kainulainen, P. Scott, and C. Weniger, Phys. Rev. D **88**, 055025 (2013); **92**, 039906(E) (2015).
[47] M. S. Turner, Phys. Rep. **197**, 67 (1990).
[48] J. Alexander *et al.*, arXiv:1608.08632.
[49] P. Langacker, Rev. Mod. Phys. **81**, 1199 (2009).
[50] T. Han, J. D. Lykken, and R.-J. Zhang, Phys. Rev. D **59**, 105006 (1999).
[51] J. F. Donoghue, M. M. Ivanov, and A. Shkerin, EPFL Lectures on General Relativity as a Quantum Field Theory (2017), arXiv:1702.00319.
[52] G. D'Amico, C. de Rham, S. Dubovsky, G. Gabadadze, D. Pirtskhalava, and A. J. Tolley, Phys. Rev. D **84**, 124046 (2011).
[53] V. A. Rubakov, arXiv:hep-th/0407104.
[54] V. A. Rubakov and P. G. Tinyakov, Phys. Usp. **51**, 759 (2008).
[55] D. Blas, J. Carlton, and C. McCabe, Phys. Rev. D **111**, 115020 (2025).
[56] A. I. Vainshtein, Phys. Lett. **39B**, 393 (1972).
[57] E. Babichev and C. Deffayet, Classical Quantum Gravity **30**, 184001 (2013).
[58] L. Alberte, C. de Rham, A. Momeni, J. Rumbutis, and A. J. Tolley, J. High Energy Phys. 03 (2020) 097.
[59] A. Berlin, A. J. Millar, T. Trickle, and K. Zhou, J. High Energy Phys. 05 (2024) 314.
[60] R. D. Peccei and H. R. Quinn, Phys. Rev. Lett. **38**, 1440 (1977).
[61] P. Adshead and K. D. Lozanov, J. High Energy Phys. 08 (2022) 077.
[62] S. L. Adler, Phys. Rev. **177**, 2426 (1969).
[63] J. S. Bell and R. Jackiw, Nuovo Cimento A **60**, 47 (1969).
[64] S. L. Adler and W. A. Bardeen, Phys. Rev. **182**, 1517 (1969).
[65] S. J. Brodsky, S. Gardner, and D. S. Hwang, Phys. Rev. D **73**, 036007 (2006).
[66] J.-W. Qiu and K. Watanabe, Prog. Theor. Exp. Phys. **2026**, ptag170 (2026).
[67] I. Abt *et al.* (ZEUS Collaboration), Eur. Phys. J. C **83**, 1082 (2023).
[68] H. Bossi *et al.* (Electron-Positron Alliance Collaboration), arXiv:2511.00149.
[69] T.-J. Hou *et al.*, Phys. Rev. D **103**, 014013 (2021).
[70] T. Han, Y. Ma, and K. Xie, J. High Energy Phys. 02 (2022) 154.
[71] J. P. Lees *et al.* (*BABAR* Collaboration), Phys. Rev. Lett. **125**, 181801 (2020).
[72] D. Biswas *et al.* (Belle Collaboration), Phys. Rev. D **109**, 032002 (2024).
[73] A. Accardi *et al.*, Eur. Phys. J. A **52**, 268 (2016).
[74] Y. M. Andreev *et al.* (NA64 Collaboration), arXiv:2505.14291.
[75] T. Akesson *et al.*, arXiv:2508.11833.
[76] H. Yang, in *32nd International Symposium on Lepton Photon Interactions at High Energies: Lepton-Photon 2025* (2025), arXiv:2512.13301.
[77] H. Davoudiasl, R. Marcarelli, and E. T. Neil, Phys. Rev. D **108**, 075017 (2023).
[78] R. Balkin, O. Hen, W. Li, H. Liu, T. Ma, Y. Soreq, and M. Williams, J. High Energy Phys. 02 (2024) 123.